

Bio-Derived Hierarchical 3D Architecture from Seeds for Supercapacitor Application

PRATTHANA INTAWIN,^{1,2} FARHEEN N. SAYED,^{2,3}
KAMONPAN PENGPAT,¹ JARIN JOYNER,²
CHANDRA SEKHAR TIWARY,^{2,4} and PULICKEL M. AJAYAN^{2,5}

1.—Department of Physics and Materials Science, Faculty of Science, Chiang Mai University, Chiang Mai 50200, Thailand. 2.—Department of Material Science and NanoEngineering, Rice University, Houston, TX 77005, USA. 3.—e-mail: farheensayed7@gmail.com. 4.—e-mail: cst.iisc@gmail.com. 5.—e-mail: ajayan@rice.edu

The generation and storage of green energy (energy from abundant and non-fossil) is important for a sustainable and clean future. The electrode material in a supercapacitor is a major component. The properties of these materials depend on its inherent architecture and composition. Here, we have chosen sunflower seeds and pumpkin seeds with a completely different structure to obtain a carbonaceous product. The product obtained from sunflower seed carbon is a three-dimensional hierarchical macroporous carbon (SSC) composed of many granular nanocrystals of potassium magnesium phosphate dispersed in a matrix. Contrary to this, carbon from pumpkin seeds (PSC) is revealed to be a more rigid structure, with no porous or ordered morphology. The electrochemical supercapacitive behavior was assessed by cyclic voltammetry and galvanostatic charge-discharge tests. Electrochemical measurements showed that the SSC shows a high specific capacitance of 24.9 Fg^{-1} as compared with that obtained (2.46 Fg^{-1}) for PSC with a cycling efficiency of 87% and 89%, respectively. On high-temperature cycling for 500 charge-discharge cycles at 0.1 Ag^{-1} , an improved cycling efficiency of 100% and 98% for SSC and PSC, respectively, is observed.

INTRODUCTION

Carbon-based composites are widely used as supercapacitor electrode materials because of their large specific surface area, good electrical properties, excellent thermal stability, low density, and cost. Thus, recent research has been focused on engineering the physical and chemical properties of carbon-based structures to improve their specific capacitance as well as power density.^{1–4} The high active surface area, porosity, and structural stability are a few of the key parameters governing the energy storage capability. Depending on the carbon precursors as well as on the activation methods used, carbon-based composites result in different electrochemical properties, which have been explored extensively in the last decade.^{5–8} Another approach to fine-tune these properties is by incorporation of metal oxides with various sizes and

their inherent properties (RuO_2 , NiO , MnO_2) resulting in synergetic behavior for electrical double-layer capacitors.^{9–11} On the other hand, a large amount of research efforts has been made to build 3D architectures of carbon-based nanomaterials such as CNTs and graphene in view of their extraordinary properties.^{12–14} Some of these nanostructured carbons are often obtained under very harsh conditions by means of laser, plasma ablation, or arc discharge, which usually indicates a high-energy consuming process.^{15–17}

All available fossil carbons are limited by the mining processes, which are hazardous and contaminative.¹⁸ The ever increasing demand of supercapacitor grade carbon materials brings an increasing pressure for high-throughput production by more feasible methods. To build a sustainable future, an energy source needs to be nonfossil based; ideally, it should be affordable and inexhaustible. In this search for an alternative carbon source, researchers have explored both a useful as well as a waste natural carbon source starting from banana peel to animal

Pratthana Intawin and Farheen N. Sayed have contributed equally to this article.

bone and many more.^{19–21} Few of the naturally abundant biomass resources often possess hierarchical 3D structures, which exhibit enhanced energy storage. These 3D nano-scaled architectures have the potential of providing a continuous electronic pathway to ensure the good electrical contacts among constituent materials.^{22, 23} To improve the properties further, surface functional groups or heteroatoms such as N, O, B, S, or P are reinforced to enhance the electrical conductivity by influencing the wettability and electro-active surface area of material.^{24–28} Another simple and easily scalable approach is to choose the biomaterials with either of these inherent dopants firmly incorporated in the carbon frame. In the current work, directed by the quest for utilizing waste biomass, with such architecture, sunflower and pumpkin seeds are explored. The role of the naturally embedded minerals like potassium, magnesium, and phosphorus are understood with the help of these two differently designed carbon sources. The results of an extensive microscopic and spectroscopic study reveal the structural differences in the active carbon derived from these sources. A comparative electrochemical study has been performed to understand the role of 3D structure and in situ doping in these two materials.

EXPERIMENTAL SECTION

Materials

Sunflower seed carbon (SSC) and pumpkin seed carbon (PSC) were synthesized by a one-step simple pyrolysis method. The sunflower and pumpkin seeds were burned at 900°C for 10 h with a heating rate of 5°C/min in argon Ar/H₂ (Fig. S1). A carbonaceous mass obtained after pyrolysis was ground into fine powder and subjected to further characterization and electrochemical investigations.

Characterization

The data for x-ray powder diffraction analysis was collected on an x-ray diffractometer (XRD, PANalytical X'Pert Pro MPD) in flat plate geometry, using Ni filtered Cu K α radiation. Data were collected from 10° to 60° with a step size of 0.02°. The spectroscopic data were recorded with a 532-nm wavelength laser on RENISHAW via Raman microscope and Perkin-Elmer Fourier transform infrared (FTIR) spectrometer in the wavenumber range of 3500–100 cm⁻¹. Scanning electron microscopy (SEM:FEI Quanta 400 ESEM FEG) analysis was used to identify the microstructure of samples. The TEM and HRTEM images were obtained with a JEOL 2010. A detailed composition analysis is performed using an FEG-EPMA (Electron probe micro-analyzer) (JEOL EPMA 8600).

Cell Fabrication and Electrochemical Measurements

To prepare the working electrode for the two-electrode system, 80 wt.% SSC/PSC, 10 wt.% conductive carbon, and 10 wt.% polyvinylidene fluoride

(PVDF) were mixed together in N-methyl-2-pyrrolidone (NMP) to form the homogeneous slurry that was casted on aluminum foil. A sandwich-type capacitor cell test was prepared with a pair of electrodes and a piece of circular quartz as a separator wetted with 0.5 M Na₂SO₄ as the aqueous electrolyte and 1-Ethyl-3-methylimidazolium bis-(trifluoromethylsulfonyl)-imide (EMITFSI) as the ionic liquid electrolyte. Cyclic voltammetry curves were obtained at various scan rates in a potential window of 0.05–0.7 V with 0.5 M Na₂SO₄ and 0.05–3 V with EMITFSI. GCD curves were recorded at various current densities (1, 2, 5, 10, and 20 Ag⁻¹) with both electrolytes.

RESULTS AND DISCUSSION

The interconnected 3D carbon structures obtained from sunflower seeds (SSC) had a porous nature, where many granular nanocrystals dispersed in the amorphous carbon matrix were clearly observed (Fig. S1 in the online supplemental material). Interestingly, these nanoparticles are homogeneously distributed over the carbon structure, whereas the carbon from pumpkin seeds (PSC) have no inherent morphology (Fig. S1).

The typical morphology of the sunflower seed with different magnifications shows that seed surfaces are a woody bark-like (Fig. S2a through h). The SEM micrographs of seed surface microstructures were observed as mostly reticulate, with different textures (Fig. S2b and c). The cross-sectional detailed morphologies of the hierarchical structures reveal that the structure of the architecture is composed of hierarchical cylindrical tubes at a length of hundreds of micrometers (Fig. S2e through h). These structures connect to each other to form 3D hierarchical architectures. The morphology and composition of the SSC sample were observed by SEM and EDS mapping at different magnifications (Fig. 1a–c). The carbon microstructures with significant numbers of secondary spherical particles homogeneously dispersed were observed, suggesting that a composite structure has been formed, in which the amorphous carbon phase forms a three-dimensional network, whereas the reinforced particles are isolated. Note that these particles are uniformly distributed over the amorphous carbon matrix. The elemental analysis covering a single particle showed the presence of C, Mg, K, P, and O. The major elemental component (carbon) was found to be distributed across the whole area (Fig. 1d–h). The other reinforcements (K, P, Mg, and O) are found to be concentrated at the particle's position. It confirms the composition of spherical particles with different sizes. The experimental volume fraction of particles can be basically quantified according to the area ratio of different components provided in the scanning electron micrograph (Fig. 1c). The experimental volume fraction of these particles with respect to carbon is calculated to be 36.5%.

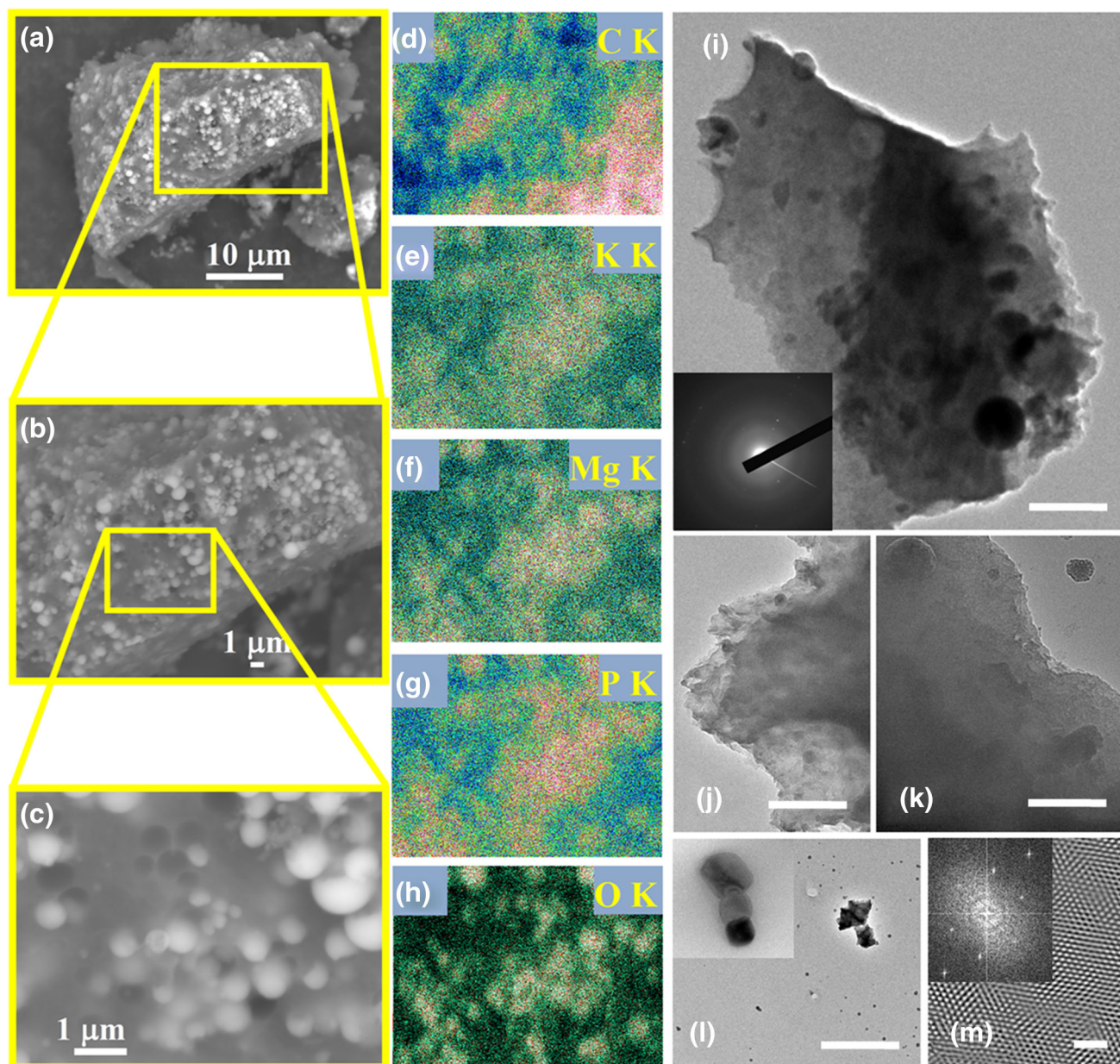


Fig. 1. (a–c) Low-magnification and high-magnification SEM images and (d–h) SEM–EDS mapping of 3D hierarchical SSC microstructure. (i) Low-magnification, bright-field TEM image ($1\ \mu\text{m}$ scale bar) and SAED pattern (amorphous carbon and crystalline spot) and (j–k) high-magnification TEM images (100-nm scale bar) of the 3D hierarchical 3D hierarchical SSC microstructure. (l) Low-magnification (scale bar $1\ \mu\text{m}$) and high-magnification TEM images of granular nanocrystals inside the SSC (100-nm size) and (m) the HRTEM image (2-nm scale bar) and SAED of a selected area in Fig. 2).

TEM images of the 3D hierarchical SSC microstructure, and the overview of the product, is consistent with the SEM results (Fig. 1i–m). A significant number of these particles is well dispersed in the amorphous carbon matrix (Fig. 1a–c). The TEM image (Fig. 1) and the selective area electron diffraction (SAED) pattern, shown in the inset, demonstrates the overall amorphous nature of the SSC sample. TEM images (Fig. 1l) with low and high magnification clearly shows embedded particles inside the SSC. The d-spacing, indexed

from the SAED pattern (Fig. 1m), confirms the existence of KMgPO_4 nano-crystallites in the amorphous carbon matrix. Detailed structural characterization using XRD, Raman, and FTIR is discussed in the online supplementary information.

In CV measurements (Fig. 2) with different scan rates ($10\text{--}200\ \text{mVs}^{-1}$) in the potential ranges from 0.05 V to 0.7 V, the characteristic rectangular shape was observed. For SSC (Fig. 2a), a larger capacitive behavior than PSC (Fig. 2b), a higher capacitance is observed. The samples of SSC and PSC displayed a

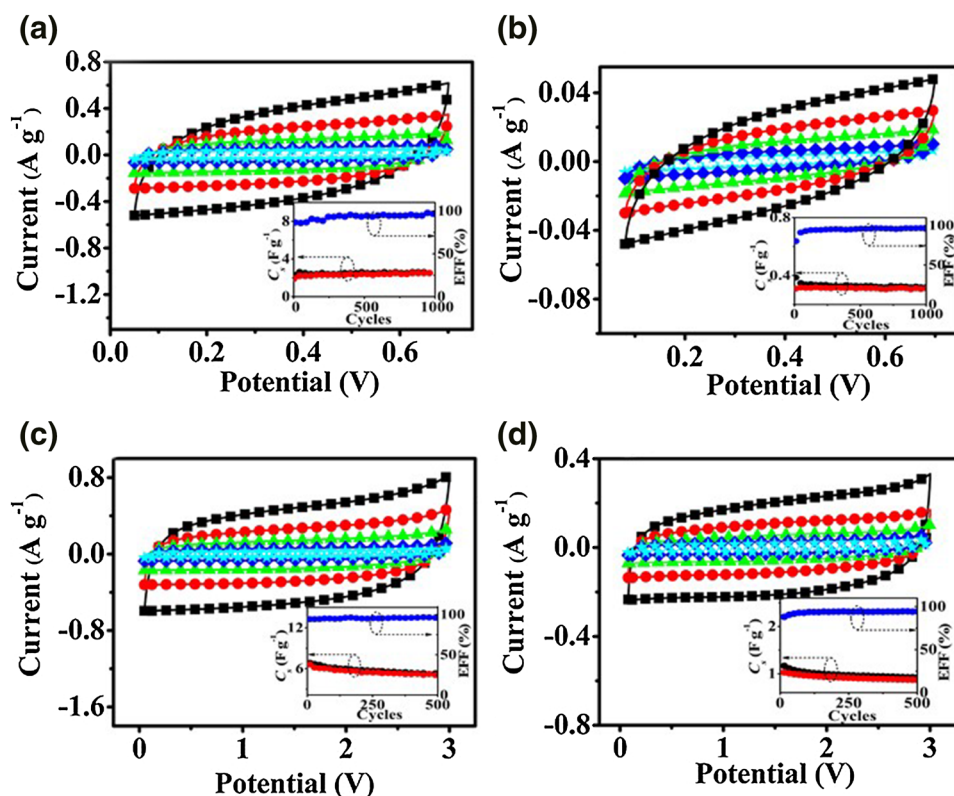


Fig. 2. CV curves with scan rates (black square, red circle, green triangle, blue diamond, and blue star = 200 mVs^{-1} , 100 mVs^{-1} , 50 mVs^{-1} , 20 mVs^{-1} , and 10 mVs^{-1}) and specific capacitance; C_s and efficiency; EFF as a function of cycle number at the current density of 0.1 Ag^{-1} of (a) SSC and (b) PSC at room temperature with $0.5 \text{ M Na}_2\text{SO}_4$ aqueous electrolyte in potential window of $0.05\text{--}0.7 \text{ V}$; (c) SSC and (d) PSC with EMITFSI ionic liquid electrolyte in potential window of $0.05\text{--}3 \text{ V}$ at 80°C (Color figure online).

specific capacitance of 24.9 Fg^{-1} and 2.46 Fg^{-1} at a scan rate of 10 mVs^{-1} , respectively. Although capacitance loss can be observed when increasing the scan rate from 10 mVs^{-1} to 200 mVs^{-1} for both samples, the SSC electrode still demonstrated a specific capacitance of as high as 13.25 Fg^{-1} . The GCD was also performed and shown in inset of Fig. 2a and b. At a constant current of 0.1 Ag^{-1} , a stable performance was observed for 1000 cycles. The observed coulombic efficiencies are 87% and 89% for SSC and PSC, respectively.

Along with aqueous electrolyte, ionic liquid EMITFSI was also used to make the same type of two-electrode sandwich cell. The CV measurements (Fig. S4a through c) at varying scan rates ($10\text{--}200 \text{ mVs}^{-1}$) in the potential ranges from 0.05 V to 3 V at RT shows the nearly rectangular shape of the plots. Owing to the less conducting nature of the ionic liquids, here current is observed as less compared with in the aqueous electrolyte. It is still interesting to observe that SSC shows better performance with EMITFSI also. Charge–discharge behavior at a constant current is shown in Fig. S4b through d. It is clearly evident that with EMITFSI, the coulombic efficiency is dramatically improved as observed from the stable nature of the charge–discharge profile. At an elevated temperature of 60°C , the viscosity of ionic liquid drops while

increasing the diffusivity into carbon matrix as well as while increasing the conductivity. Hence, the overall capacitance is found to be increased at lower scan rate. Nevertheless, as the scan rate increases, the kinetics of ionic movement become so rapid that the capacitive property of material is decreased and, hence, the values decrease in comparison with the values obtained for RT cells. In 500 charge/discharge cycles at 0.1 Ag^{-1} , the cycling efficiency is 100% and 98% for SSC and PSC, respectively.

With promising results at an ambient temperature condition, the samples were further explored for high-temperature performance. The samples of SSC and PSC displayed a specific capacitance of 24.5 Fg^{-1} and 3.87 Fg^{-1} at a scan rate of 10 mVs^{-1} , respectively. The cyclic efficiency of 96% and 93% for SSC and PSC, respectively, over 500 charge/discharge cycles at 0.1 Ag^{-1} is observed.

The rate capability and observed specific capacitance of the SSC electrode at RT (Fig. 3a) is monitored at the specific discharge/charge densities of 1 Ag^{-1} , 2 Ag^{-1} , 5 Ag^{-1} , and 10 Ag^{-1} . The specific capacitances obtained were 2.72 Fg^{-1} , 2.25 Fg^{-1} , 1.48 Fg^{-1} , and 0.79 Fg^{-1} , respectively. At 80°C (Fig. 3b), the specific capacitances were changed to 4.62 Fg^{-1} , 3.38 Fg^{-1} , 1.37 Fg^{-1} , and 0.16 Fg^{-1} , respectively. Such an excellent rate performance suggested that the SSC electrodes could be fully

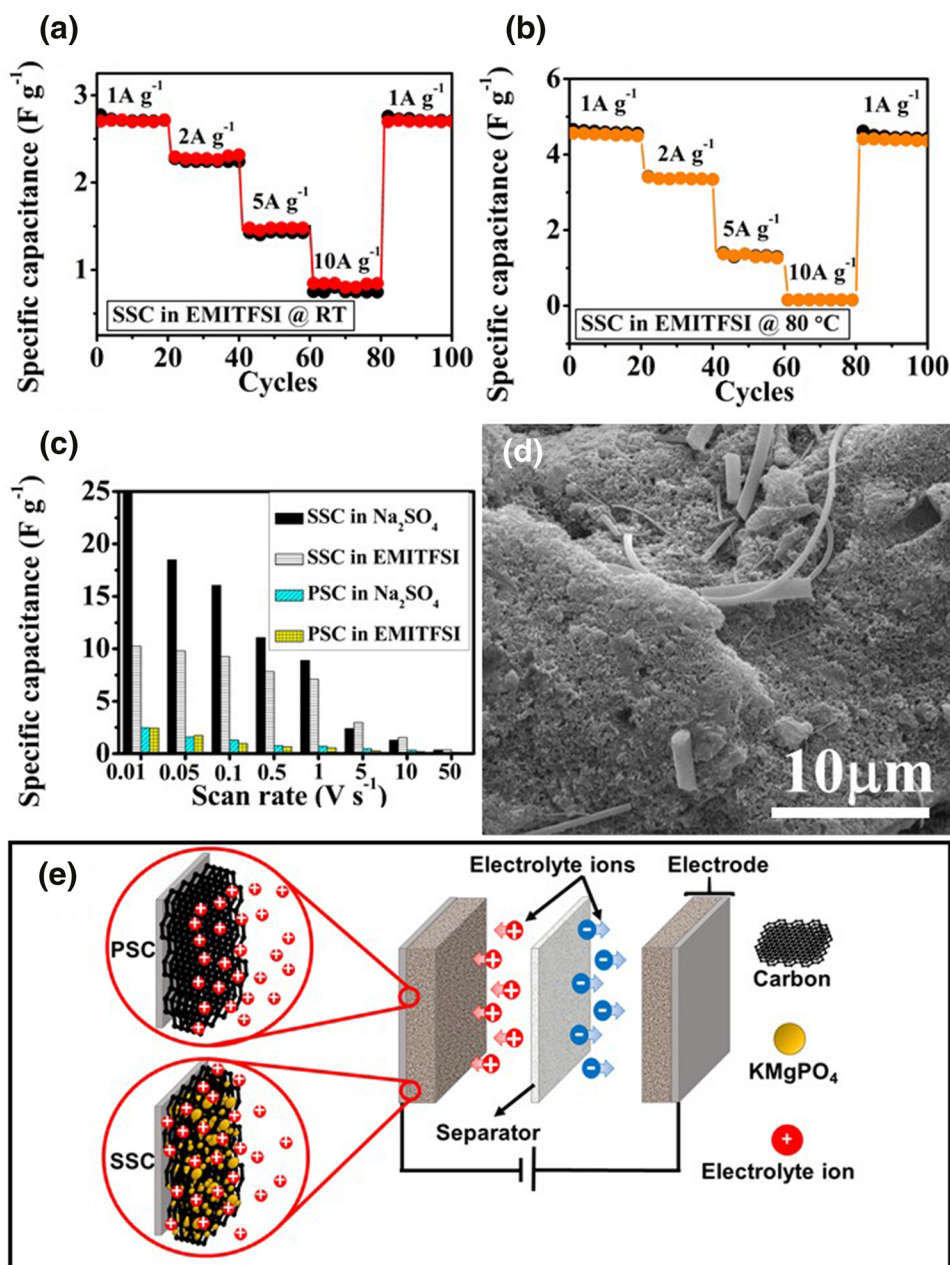


Fig. 3. Cycle stability at (a) room temperature (b) 80 °C of SSC at different current densities in EMITFSI ionic liquid electrolyte; (c) Comparison of the two samples under investigation with different electrolytes at RT; (d) SEM images of SSC with 0.5 M Na₂SO₄ aqueous electrolyte after 500 cycles of charge–discharge. (e) Schematic of insight of improved performance for SSC over PSC supercapacitor.

charged rapidly and can be explored as a high-rate supercapacitor with promising properties at ambient as well as at high temperatures. A comparative quantification plot of the data obtained is summarized in Fig. 3c. In accordance with our hypothesis of effective in situ substitution in the carbon matrix, improved performance was obtained as a result of increased active sites at the carbon particle, which is clearly reflected in electrochemical performance. The morphology of the cycled SSC electrodes was compared with the uncycled electrode sample using SEM (Fig. 3d) to observe the long cycling effect, if

any. After a 1000-cycle test, the SEM of SSC electrodes demonstrated no significant change, suggesting that the morphology of the SSC sample remains unaltered during the cycling. As a result of the long-range continuous hierarchical structure and high KMgPO₄ phase contents, SSC is proved to be better carbon material with a high specific capacitance of 24.9 Fg⁻¹ at a scan rate of 10 mVs⁻¹ and excellent reversibility with cycling efficiency of 87% after 1000 cycles at a current density of 0.1 mA g⁻¹ in 0.5 M Na₂SO₄. At 80 °C, the SSC still shows a high specific capacitance of 24.5 Fg⁻¹ at a

scan rate of 10 mVs^{-1} and excellent reversibility with cyclic efficiency of 100% after 500 cycles at a current density of 10 mA g^{-1} in EMITFSI.

In an attempt to extract the useful carbon materials from waste and organic sources available, we have successfully used the sunflower and pumpkin seeds. Instead of commonly employed harsh chemical treatments, the simple method was employed. We have observed a good rate capability behavior with a scan rate from as low as 10 mV to a higher scan rate of 200 mV . The positive aspect of the bigger particle size achieved was the high-temperature performance of materials, which in the case of nano materials could be very poor. Herein, in another attempt, it is also revealed that the selection of carbon source in terms of their inherent composition can play a beneficial role. The natural constituents of sunflower seed, potassium, magnesium, and phosphorous are transformed into secondary sites by forming a phosphate structure into the carbon matrix. These secondary structure then itself can act as the active site for the ions from electrolyte/analyte (Fig. 3e) and further facilitate the total activity of the materials. In the case with optimized synthesis, to get a reduced particle size and modified network of structure, these active sites will be throughout the channels providing a homogenous path for ion transfer/diffusion. Hence, we believe that the results of the present study will further attract the attention of researchers toward development of similar economical and environmentally friendly approaches.

CONCLUSION

In summary, we have demonstrated that a common biomass, the sunflower and pumpkin seeds, can be converted into a carbon, and reinforced with a potassium magnesium phosphate for the supercapacitor. The 3D hierarchical macroporous carbon composed of many granular nanocrystals of potassium magnesium phosphate dispersed in the amorphous carbon matrix is extremely stable during the long-life charge/discharge process; as a consequence, the capability and cyclic stability are greatly improved. When evaluated as an active material, it demonstrated a high specific capacitance and excellent cyclic stability. Such capacitive performance makes the carbon-KMgPO₄ composite of SSC a promising electrode material for the supercapacitor.

ACKNOWLEDGEMENTS

Pratthana Intawin would like to thank Chiang Mai University and the Royal Golden Jubilee Ph.D. Program for financial support. C.S.T. and P.M.A. acknowledge the funding from the U.S. Department of Defense: U.S. Air Force Office of Scientific Research for the Project MURI: "Synthesis and Characterization of 3-D Carbon Nanotube Solid Networks" Award No. FA9550-12-1-0035.

ELECTRONIC SUPPLEMENTARY MATERIAL

The online version of this article (doi:10.1007/s11837-017-2406-7) contains supplementary material, which is available to authorized users.

REFERENCES

1. B.E. Conway, *Electrochemical Supercapacitors; Scientific Fundamentals and Technological Applications* (New York: Plenum Press, 1999).
2. Z.B. Lei, N. Christov, L.L. Zhang, and X.S. Zhao, *J. Mater. Chem.* 21, 2274 (2011).
3. Y. Korenblit, M. Rose, E. Kockrick, L. Borchardt, A. Kvit, S. Kaskel, and G. Yushin, *ACS Nano* 4, 1337 (2010).
4. D.W. Wang, F. Li, M. Liu, G.Q. Lu, and H.M. Cheng, *Angew. Chem. Int. Ed. Engl.* 47, 373 (2008).
5. B.E. Conway, V. Birss, and J. Wojtowicz, *J. Power Source* 66, 1 (1997).
6. E. Frackowiak and F. Beguin, *Carbon* 39, 937 (2001).
7. K. Kierzek, E. Frackowiak, G. Lota, G. Gryglewicz, and J. Machnikowski, *Electrochim. Acta* 49, 1169 (2004).
8. E. Raymundo-Pinero, F. Leroux, and F. Beguin, *Adv. Mater.* 18, 1877 (2006).
9. J.R. Zhang, D.C. Jiang, B. Chen, J.J. Zhu, L.P. Jiang, and H.Q. Fang, *J. Electrochem. Soc.* 148, A1362 (2001).
10. G.H. Yuan, Z.H. Jiang, A. Aramata, and Y.Z. Gao, *Carbon* 43, 2913 (2005).
11. T. Morishita, Y. Soneda, T. Tsumura, and M. Inagaki, *Carbon* 44, 2360 (2006).
12. A.P.P. Alves, R. Koizumi, A. Samanta, L.D. Machado, A.K. Singh, D.S. Galvao, G.G. Silva, C.S. Tiwary, and P.M. Ajayan, *Nano Energy* 31, 225 (2017).
13. S.P. Jose, C.S. Tiwary, S. Kosolwattana, P. Raghavan, L.D. Machado, C. Gautam, T. Prasankumar, J. Joyner, S. Ozden, D.S. Galvao, and P.M. Ajayan, *RSC Adv.* 6, 93384 (2016).
14. S. Vinod, C.S. Tiwary, L.D. Machado, S. Ozden, R. Vajtai, D.S. Galvao, and P.M. Ajayan, *Nanoscale* 8, 15857 (2016).
15. T.W. Ebbesen and P.M. Ajayan, *Nature* 358, 220 (1992).
16. G.N. Churilov, *Instrum. Exp. Tech.* 43, 1 (2000).
17. K.S. Kim, Y. Zhao, H. Jang, S.Y. Lee, J.M. Kim, K.S. Kim, J. Ahn, P. Kim, J. Choi, and B.H. Hong, *Nature* 457, 706 (2009).
18. E.R. Bobicki, Q. Liu, Z. Xu, and H. Zeng, *Prog. Energy Combust. Sci.* 38, 302 (2012).
19. M.S. Balathanigaimani, W.G. Shim, M.J. Lee, C. Kim, J.W. Lee, and H. Moon, *Electrochim. Commun.* 10, 868 (2008).
20. S.G. Lee, K.H. Park, W.G. Shim, and M.S. Balathanigaimani, *J. Ind. Eng. Chem.* 17, 450 (2011).
21. X. Li, W. Xing, S.P. Zhuo, J. Zhou, F. Li, S.Z. Qiao, and G.Q. Lu, *Bioresour. Technol.* 102, 1118 (2011).
22. Z. Li, L. Zhang, B.S. Amirkhiz, X. Tan, Z. Xu, H. Wang, B.C. Olsen, C.M.B. Holt, and D. Mitlin, *Adv. Energy Mater.* 2, 431 (2012).
23. B.G. Choi, M. Yang, W.H. Hong, J.W. Choi, and Y.S. Huh, *ACS Nano* 6, 4020 (2012).
24. D. Hulicova-Jurcakova, M. Sereydyh, G.Q. Lu, and T.J. Bandoz, *Adv. Funct. Mater.* 19, 438 (2009).
25. L.F. Chen, X.D. Zhang, H.W. Liang, M. Kong, Q.F. Guan, P. Chen, Z.Y. Wu, and S.H. Yu, *ACS Nano* 6, 7092 (2012).
26. D. Hulicova-Jurcakova, A.M. Puziy, O.I. Poddubnaya, F. Suárez-García, J.M.D. Tarascon, and G.Q. Lu, *J. Am. Chem. Soc.* 131, 5026 (2009).
27. M. Zhong, E.K. Kim, J.P. McGann, S.E. Chun, J.F. Whitacre, M. Jaroniec, K. Matyjaszewski, and T. Kowalewski, *J. Am. Chem. Soc.* 134, 14846 (2012).
28. Z. Li, Z. Xu, X. Tan, H. Wang, C.M.B. Holt, T. Stephenson, B.C. Olsen, and D. Mitlin, *Energy Environ. Sci.* 6, 871 (2013).